JCI The Journal of Clinical Investigation

Anti-retroviral therapy does not reduce tuberculosis reactivation in a tuberculosis-HIV co-infection model

Shashank R. Ganatra, Allison N. Bucsan, Xavier Alvarez, Shyamesh Kumar, Ayan Chatterjee, Melanie Quezada, Abigail I. Fish, Dhiraj K. Singh, Bindu Singh, Riti Sharan, Tae-Hyung Lee, Uma Shanmugasundaram, Vijayakumar Velu, Shabaana A. Khader, Smriti Mehra, Jyothi Rengarajan, Deepak Kaushal

J Clin Invest. 2020. https://doi.org/10.1172/JCI136502.

Research In-Press Preview AIDS/HIV Infectious disease

Graphical abstract

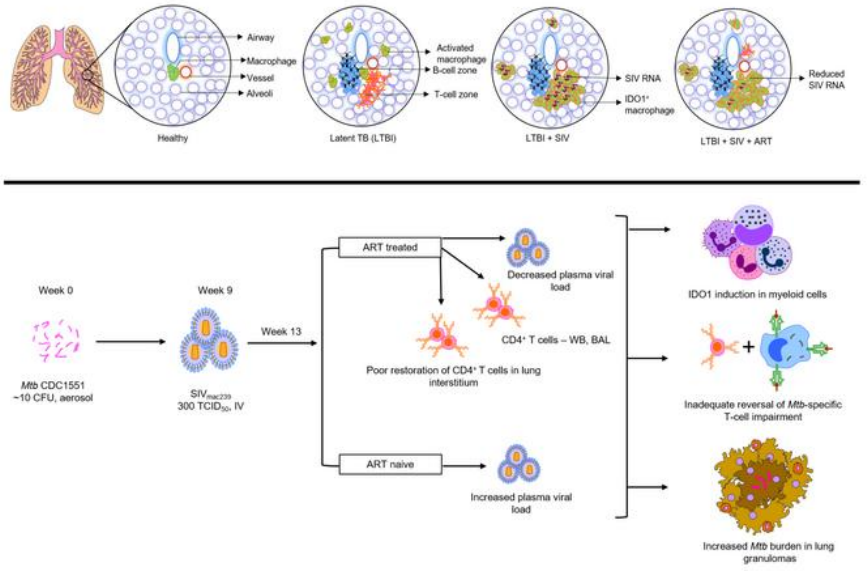

Find the latest version:

https://jci.me/136502/pdf

Title: Anti-retroviral therapy does not reduce tuberculosis reactivation in a tuberculosis-HIV co-infection model

Authors: Shashank R. Ganatra[1], Allison N. Bucşan[2$], Xavier Alvarez[1,2], Shyamesh Kumar[1], Ayan Chatterjee[1], Melanie Quezada[3,4], Abigail Fish[1], Dhiraj Kumar Singh[1], Bindu Singh[1], Riti Sharan[1], Tae-Hyung Lee[1], Uma Shanmugasundaram[3,4], Vijayakumar Velu[3,4], Shabaana A. Khader[5], Smriti Mehra[2], Jyothi Rengarajan[3,4,6*#] Deepak Kaushal[1*#]

Affiliations: [1]Southwest National Primate Research Center, Texas Biomedical Research Institute, San Antonio, TX; [2]Tulane National Primate Research Center, Covington, LA; [3]Emory Vaccine Center; and [4]Yerkes National Primate Research Center, Emory University School of Medicine, Atlanta, GA; [5]Department of Molecular Microbiology, Washington University School of Medicine in St Louis, St Louis, MO; [6]Department of Medicine, Division of Infectious Diseases, Emory University School of Medicine, Atlanta, GA

[#]Contributed equally

*To whom correspondence may be addressed: Deepak Kaushal, PhD, Director, Southwest National Primate Research Center, Texas Biomedical Research Institute, 8715 W. Military Drive, San Antonio, TX, 78227; Email: dkaushal@txbiomed.org; Tel. (210)258-9445; AND Jyothi Rengarajan, PhD, Emory Vaccine Center, 954 Gatewood Rd, Room 1022, Atlanta, GA; Email: jrengar@emory.edu; Tel. +1(404) 727-8174.

[$]Current address: Vaccine Research Center, National Institutes of Allergy and Infectious Diseases, NIH, Bethesda, MD, 20814.

Statement on conflict of interests: "The authors declare that no conflict of interest exists."

Abbreviations: cART, combination Anti-retroviral Therapy; ATB, active TB; BAL, bronchoalveolar lavage; CFU, Colony Forming Unit; CRP, C-reactive protein; CXR, thoracic radiograph; iBALT, inducible bronchus-associated lymphoid tissue; LTBI, latent tuberculosis infection; *Mtb*, *Mycobacterium tuberculosis*; NHP, non-human primate; PBMC, peripheral blood mononuclear cell; BrLN, Bronchial lymph node; PLHIV, People living with HIV; SIV, Simian Immunodeficiency Virus; TB, tuberculosis; TST, tuberculin skin test.

Abstract.

While the advent of combination antiretroviral therapy (ART) has significantly improved survival, tuberculosis (TB) remains the leading cause of death in the HIV-infected population. We employed *Mtb*/Simian Immunodeficiency Virus (SIV) co-infected macaques to model *Mtb*/HIV co-infection and study the impact of ART on TB reactivation due to HIV-infection. While ART significantly reduced viral loads and increased $CD4^+$ T cell counts in blood and BAL samples, it did not reduce the relative risk of SIV-induced TB reactivation in ART treated macaques in the early phase of treatment. $CD4^+$ T cells were poorly restored specifically in the lung interstitium, despite their significant restoration in the alveolar compartment of the lung as well as in the periphery. IDO1 induction in myeloid cells in the iBALT likely contributed to dysregulated T cell homing and impaired lung immunity. Thus, while ART is indispensable in controlling viral replication, $CD4^+$ T cells restoration, and preventing opportunistic infection, it appears inadequate in reversing clinical signs of TB reactivation during the relatively short duration of ART administered in this study. This warrants modeling concurrent treatment of TB and HIV to potentially reduce the risk of reactivation of TB due to HIV to inform treatment strategies in patients with *Mtb*/HIV co-infection.

Introduction.

The modern combination antiretroviral therapy (cART) regimen, which is known for its high efficacy and reduced toxicity, has significantly improved life expectancy in people living with HIV (PLHIV). Yet co-morbidities such as tuberculosis (1) contribute significantly to all-cause mortalities in ART-adherent populations (2, 3) and the World Health Organization (WHO) reported 215,000 TB-associated deaths in HIV-infected populations in 2018. This suggests that

ART fails to completely restore protective immunity to *Mycobacterium tuberculosis* (*Mtb*). Despite scale-up efforts to facilitate ART accessibility to around 84% of notified PLHIV (4), an increased risk of mycobacterial infections with an associated risk of mortality (5) remains high within the first year of treatment in resource-limited settings (5, 6). Additionally, a paradoxical worsening of tuberculous symptoms has been shown to occur soon after the initiation of ART in HIV-infected TB patients (7, 8). This is followed by a significant decline in reactivation risk with increased duration of adherence to ART and associated improvements in $CD4^+$ T cell counts. Although ART is associated with a significant reduction in the incidence of TB irrespective of $CD4^+$ T cell count status (9), the lifetime risk of TB reactivation in ART-adherent cases remains four to seven-fold higher than in HIV-uninfected populations (9, 10). CD4 T cell dysfunction and chronic immune activation are reported alongside CD4+ T cell restoration in ART adherent PLHIV(11-13). Lung pathology was reported in 75-85% of HIV/AIDS autopsies (14) and the plethora of opportunistic infections that can arise in the lung of HIV-infected individuals suggests that their lung environments remain immunologically impaired. Thus, understanding the components of TB immunity that remain impaired following HIV co-infection and ART treatment will provide insights into improving treatments for TB and HIV co-infection.

Previously, we have shown that a nonhuman primate (rhesus macaque) model of *Mtb*/SIV co-infection effectively recapitulate many aspects of human disease, including productive SIV infection, $CD4^+$ T cell depletion, *Mtb* reactivation, and chronic immune activation (15-20). Here we extend this model to study the impact of ART on viral replication, $CD4^+$ T cell restoration in various tissue compartments, chronic immune activation, and TB reactivation. Our results indicate that while ART effectively and rapidly controls SIV replication in co-infected macaques, leading

to $CD4^+$ T cell restoration, it does not decrease SIV-induced TB reactivation during the period studied.

Results.

Clinical correlates of TB reactivation in ART-treated NHPs with *Mtb*/SIV co-infection:

Sixteen Indian-origin mycobacteria- and SPF-4-naïve rhesus macaques (*Macaca mulatta*) that were infected with ~10 CFUs of *Mtb* CDC1551 via aerosol (15, 21), converted to positive tuberculin skin tests (TSTs) after 3 weeks of *Mtb* exposure (Table S1), confirming *Mtb* infection and remained devoid of signs and symptoms of TB disease for up to 9 weeks after *Mtb* infection were considered to have latent TB infection (LTBI), and used for further perturbations (Additional details in Supplemental Methods and Table S1). A subset of the animals with established LTBI (n=12) was challenged with 300 $TCID_{50}$ $SIVmac_{239}$ via the intravenous route (15, 17, 22). Infection with SIV was confirmed by plasma viral load performed at longitudinal time points, and at 13 weeks post-*Mtb* infection, four animals were initiated on WHO-recommended ART regimen consisting of dolutegravir 2·5 mg ml^{-1} (DTG) and two nucleoside reverse transcriptase inhibitors tenofovir disoproxil 20 mg ml^{-1} (PMPA), and emtricitabine 30 mg ml^{-1} (FTC) once daily through a single subcutaneous injection (23). The three experimental groups namely, LTBI, ART-naïve, and ART (Fig 1A) were studied longitudinally for their clinical and pathological features and their immune responses.

ART-treated animals showed rapid and significant (~3-log) decline ($p < 0.00001$) in plasma SIV viral loads compared to untreated controls within weeks of ART initiation (Fig 1B). Despite the decline in SIV viral loads, however, there was no improvement in survival with a relative risk of

TB reactivation in the ART-treated group (RR 1.23, 95% CI 0.97-1.5) compared to ART-naïve controls (Fig 1C). None of the animals in the LTBI group (n=4) showed any clinical or pathological signs of TB at any point during the length of the study and were euthanized at week 24. Clinical parameters that were monitored weekly, such as changes in weight and body temperature (Fig S1A-B), showed no significant differences between the groups. We have previously shown that elevated serum CRP levels correlated with lung *Mtb* burdens irrespective of *SIV* infection status (20). Serum CRP was not detected in the LTBI group, consistent with the low bacterial burdens in these animals. However, CRP levels were significantly elevated ($p = 0{\cdot}0248$) in both ART-naïve and ART-treated groups with *Mtb*/SIV co-infection at the necropsy endpoint relative to the pre-SIV infection time point (week 9). Furthermore, no differences in serum CRP levels were observed in the ART-naïve and ART groups ($p = 0{\cdot}9073$) at necropsy (Fig 1D). Viral loads in the acellular BAL fluid, obtained at necropsy, also recorded significantly decreased viral loads ($p = 0{\cdot}0353$) relative to controls (Fig 1E). Using the RNAscope *in situ* hybridization (ISH) assay, which detects intracellular SIV RNA targets, and performed a semi-quantitative analysis based upon the counting of the number of cells with discrete intracellular punctate red dots. The semi-quantitative scores were (mean±SEM) 0.833±0.16, and 0±0 for lungs, 4±0, and 2.4 ± 0.4 for spleen, 2.83±1.16, and 2.1±0.29 for lymph node in ART-naïve (n=3) and ART (n=3) groups respectively, and were not significantly different. We found that ART-naïve animals displayed a high density of SIV $vRNA^+$ cells in lymphocyte-rich structures such as germinal centers in spleen and bronchial lymph node (BrLN) and periarterial lymphatic sheaths in the spleen (Fig 1F). However, there were few $vRNA^+$ cells in lung tissue, localized in peribronchovascular bronchus-associated lymphoid tissue (BALT), and rarely in the lung parenchyma, consistent with findings from various studies reporting that lungs harbor few productively-infected cells during acute SIV infection (24, 25).

Besides, as early as two weeks after ART therapy initiation, there were substantially lower numbers of SIV vRNA^{+} cells reported in germinal centers of spleen and BrLN, with minimal change in the lung.

***Mtb* burden and associated lung pathology during ART therapy in *Mtb*/SIV co-infection:**

The *Mtb* burdens in LTBI, ART-naïve, and ART-treated animals by plating BAL, lungs, BrLN, and spleen tissue collected at necropsy. BAL samples from the LTBI group had no detectable tubercle bacilli, however, significantly higher *Mtb* burdens ($p = 0{\cdot}0014$) were present in SIV co-infected animals irrespective of ART treatment. Similarly, SIV co-infected animals from both ART-naïve and ART-treated groups had higher *Mtb* burdens in lungs ($p = 0{\cdot}0464$), BrLN ($p = 0{\cdot}0067$) and spleen ($p = 0{\cdot}0402$) compared to the LTBI group, with no significant differences between ART-naive and ART-treated groups ($p = 0{\cdot}8568$, $p = 0{\cdot}6577$, $p = 0{\cdot}2437$, respectively) (Fig 2A-E). While granulomas are a hallmark of TB pathology, lung granulomas are known to be heterogeneous for cellular composition, bacterial burden, and gross pathology (26). At necropsy, lung resected from the macaques were manually dissected to macroscopically identify granulomas and study their gross, mycobacterial, and immune characteristics. We found a significantly higher bacterial burden ($p = 0{\cdot}0002$) in granulomas from SIV co-infected animals compared to LTBI animals with ART offering no significant reduction ($p = 0{\cdot}1348$) in granuloma *Mtb* CFU. Using the grid overlay technique described previously (27), serial lung sections were assessed for the number of lesions in each field to generate an arbitrary score corresponding to the percentage of lung involvement (Fig 2F). Animals with *Mtb*/SIV co-infection showed significantly higher numbers of lesions ($p= 0{\cdot}0240$) compared to LTBI with ART-treated animals having scores comparable to ART-naive controls ($p= 0{\cdot}99$). Gross pathology (Fig 2G) shows that reactivated

161 animals harbored numerous, large granulomas and H&E staining shows confluent granulomas
162 with necrotic cores in both ART-naïve and ART-treated groups.
163
164 **Differential CD4$^+$ T cell restoration in alveolar and interstitial compartments after ART**
165 **therapy in *Mtb/SIV* co-infection of NHPs.**
166 CD4$^+$ T cell depletion in the setting of SIV infection and its role in TB reactivation has been
167 actively studied (15, 21). We studied the effect of ART on CD4$^+$ T cells in various tissues using
168 multiparameter flow cytometry. Compared to ART-naive controls, ART-treated animals showed
169 significantly higher CD4$^+$ T cells in whole blood ($p = 0{\cdot}0427$), BAL ($p = 0{\cdot}0009$), BrLN ($p =$
170 $0{\cdot}0229$) and spleen ($p = 0{\cdot}0174$) (Fig 3A-E), indicating that ART was able to significantly restore
171 CD4$^+$ T cells in these compartments. In contrast, minimal restoration of CD4$^+$ T cells was observed
172 in the lung interstitium (supporting tissue that includes alveolar epithelium, pulmonary capillary
173 endothelium, along with perivascular, and perilymphatic tissues) following ART (Fig 3C, F, G).
174 We have previously reported a role for interstitial CD4$^+$ T cell depletion in the dissemination of
175 TB (28). Thus, the lack of, or delay in, restoration of interstitial CD4$^+$ T cell in the lungs of ART-
176 treated animals in our study, is consistent with reactivation to TB that occurred despite ART.
177 Chronic immune activation is associated with HIV and TB/HIV co-infection and can result in
178 delayed functional recovery of the immune system and accelerate progression to AIDS (29). We
179 found no significant differences in the frequencies (Fig S2A-F and S3A-B) of HLA-DR$^+$ CD4$^+$ T
180 cells, PD-1$^+$ CD4$^+$ T cells, CXCR3$^+$ CD4$^+$ T cells, and CCR6$^+$ CD4$^+$ T cells, in blood and BAL
181 samples from ART-naïve and ART treated groups. However, CD69$^+$CD4$^+$ T cell levels, a marker
182 of early activation in response to *Mtb* antigen (21, 30), were higher in BAL samples of the ART-
183 treated group compared to ART-naïve and LTBI groups. There was a significant increase in the

184 frequency of CXCR3+ CCR6+ CD4+ T cells in ART treated animals. CD4+ T cells co-expressing
185 CXCR3 and CCR6 are reported to be preferentially enriched with HIV DNA in PLHIV on
186 HAART(31). There was a selective expansion of CXCR3+CD4+ and CCR6+CD4+ T cell
187 populations, within 2 weeks of cART initiation Fig (S4A-B). Our findings are in line with a recent
188 report suggesting an increase in expression of CXCR3+CCR6+CD4+ T cells are associated with
189 the onset of TB-IRIS in HIV patients recently initiated on HAART (32).
190 We observed an increased presence of $CD68^{+}CD163^{+}$ macrophages in the lung section of *Mtb*/SIV
191 co-infected animals, though the differences between ART-naïve and ART groups were not
192 significant (p=0.2654) (Fig S6). This increase in myeloid population can be due Type I IFN
193 mediated proliferation and trafficking of *Mtb*-permissive innate immune cells contribute to the
194 exacerbation of TB disease (33).
195
196 **Dysregulation in homing of $CD4^{+}$ T cells to iBALT in lung interstitium of *Mtb/SIV* co-**
197 **infected macaques.**
198 The presence of effector bronchus-associated lymphoid tissue (iBALT) is known to contribute
199 towards protection against *Mtb* and prevent reactivation of latent TB (34). These iBALT structures,
200 formed in the lungs of *Mtb* infected macaques, provide an environment for B cell maturation,
201 antigen-specific memory effector T cells within the tissue (35). iBALT structures are highly
202 organized lymphoid aggregates consisting of B cell zones, serving as a germinal center and T cell
203 zones, harboring $CD4^{+}$ and $CD8^{+}$ T cells along with dendritic cells and high endothelial venules
204 (36, 37). $CD4^{+}$ effector memory T cells residing in these iBALTs are targeted by SIV resulting in
205 their depletion and poor reconstitution despite successful control of viral replication by ART (38).
206 We have previously demonstrated that iBALT persisted in the lungs of rhesus macaques in the

setting of *Mtb/SIV* co-infection even when $CD4^+$ T cells are depleted. Moreover, iBALT structures occupied a higher percentage of lung area in non-reactivators compared to reactivators, suggesting that the presence of iBALT correlates with protective immunity against *Mtb* reactivation in the setting of *Mtb/SIV* co-infection (15, 39). In this study, we examined iBALT structures in the lung by using immunohistochemistry. We observed a predominance of $CD68^+CD163^+$ macrophages (Fig 4A) phagocytosing necrotic SIV infected cells in the T cell zone, which is typically occupied by $CD4^+$ T lymphocytes in lesions from macaques with LTBI. The presence of these productively infected macrophages and myeloid cells have been shown to serve as a reservoir for SIV in ART-suppressed macaques and are associated with high levels of immune activation (40). We have previously shown in our model of *Mtb*/SIV co-infection, through BrdU labeling, that high turnover of macrophages correlates with TB reactivation (20). Studies have shown that CD4+ T cell depletion, post SIV infection, significantly increase in viral replication in macrophages and other antigen presenting cells (41). In the face of ART, these SIV infected macrophages serve as a reservoir by harboring latent viral genomes and contribute to viral rebound upon ART interruption (40). High turnover of macrophages contributes to macrophage persistence as antigen-presenting cell and drives chronic immune activation (42). Furthermore, a recent study also suggests of the synergy between *Mtb* and SIV within lung granuloma facilitate Mtb bacterial dissemination and growth thus contributing to TB reactivation (43). Thus, our work suggests a significant dysregulation in the reconstitution of iBALT structures proximal to granulomas despite ART, and this may be one of the major mechanisms by which immune function remains impaired in *Mtb*/HIV co-infected individuals.

Further investigation of macrophages and myeloid-derived cells in the T cell zone of BALT showed that they express indoleamine 2,3-dioxygenase (IDO1). IDO1-expressing macrophages in

granulomatous lesions (Fig 4B). Our previous studies in the macaque model of *Mtb* infection showed IDO-expressing cells in the macrophage-rich layer of granulomas, which likely serves to prevent optimal interactions between $CD4^+$ T cells and *Mtb*-infected antigen-presenting cells. Moreover, increased expression of IDO1 correlated with *Mtb* bacterial burden and IDO1 expression was also associated with poorly formed iBALT. Our lab has previously reported that blocking IDO1 activity resulted in re-organization of granulomas and granuloma-associated iBALT structures, resulting in improved *Mtb* clearance (44). IDO1 is an immunoregulatory enzyme known to induce apoptosis of effector $CD4^+$ T cells and promote T regulatory cells. Thus, expression of IDO in macrophages (Fig 4C), $CD141^+$ tolerogenic dendritic cells (Fig 4D), and other myeloid lineage cells in ART-treated animals may promote dysregulated homing of $CD4^+$ T cells in the T cell zone of the iBALT and poor restoration of $CD4^+$ T cells in the lung interstitium. Furthermore, our model can serve as a resource to test efficacy of various IDO1 modulating agents in preventing TB reactivation, and ameliorating chronic immune activation.

Discussion.

While the macaque model of *Mtb*/HIV co-infection has been extensively utilized, ours is the first report of implementing ART in this model system. Our results suggest that ART significantly reduces SIV viral loads in all tissue compartments. Furthermore, significant restoration of $CD4^+$ T cell levels is observed in the periphery, the alveolar compartment, as well as in extrapulmonary tissues. We clearly show, however, that ART failed to reconstitute $CD4^+$ T cells in the lung tissue during the shorter duration of ART administered in this study. This exhibits a strength of our model system, since extensive interrogation of the lung tissue is virtually impossible in human patients. Accordingly, ART was unable to prevent SIV-induced reactivation of LTBI in the early phase of

treatment. As in humans, the *Mtb*/SIV co-infection/ART model in rhesus macaques recapitulated the efficacy of ART in viral load reduction and $CD4^+$ T cell reconstitution. A meta-analysis reports, 18% pooled incidence of tuberculosis-associated IRIS in PLHIV initiated on ART(45). Thus, while ART prevents TB in many PLHIV, yet a significant minority of such individuals develop TB. Our results suggest that imprecise or dysregulated restoration of $CD4^+$ T cells to the lung may play a significant role in this process. Our success in being able to model a more wide-spread failure of LTBI maintenance may be due to the use of a system where high doses (300 TCID50) of the virus were used for co-infection via the systemic, intravenous route. The use of a physiologically relevant low dose and mucosal route for SIV co-infection along with the use of extremely low-doses of *Mtb* for infection necessary to generate LTBI in our model would, however, render our model cost-prohibitive and statistically underpowered. Although in our model of *Mtb*/SIV co-infection, we challenged latent tuberculosis macaque with SIV to study the role of SIV infection on *Mtb* specific CD4+ T- cell immunity, we understand that the sequence of infection can be reverse in areas with HIV and TB syndemic. Our findings of TB reactivation with SIV challenge at nine weeks post-*Mtb* infection are in tune with findings of other groups where SIV challenge followed after 8-10 months(16) after *Mtb* infection, developed TB reactivation. Also, our model may be of value at studying recurrent TB in PLHIV, explaining the cause of relapse after anti-TB treatment completion (46) and increased susceptibility to exogenous *Mtb* reinfection after curative anti-TB therapy (47).

Our findings are consistent with available human data suggesting that initiation of ART after *Mtb*/HIV co-infection may not prevent reactivation of LTBI in all individuals (48, 49). It is, however, conceivable that coupling ART with either Isoniazid Preventive Therapy (IPT) or

Isoniazid plus Rifapentine three-month therapy (3HP), may completely or significantly prevent TB reactivation. In this regard, it is important to note that we have developed a model for LTBI treatment in macaques using 3HP (18). Furthermore, as novel treatment regimens for LTBI with greater efficacy are developed, our model could serve as the key resource to validate them. As such, our results have the potential to inform treatment approaches for the syndemic resulting from the two most important infectious diseases of humanity.

Methods:

Study approval. All the animals were housed in the Animal Biosafety level III (ABSL3) at Tulane National Primate Research Center where they were treated as per the standards recommended by Association for Assessment and Accreditation of Laboratory Animal Care (AAALAC) International and the NIH Guide for the Care and Use of Laboratory Animals. The study was approved by the IACUC of the Tulane National Primate Research Center (TNPRC) (protocols P0247R, P0324, P0295R).

Animal studies

Animal studies were performed following approved IACUC protocols at TNPRC (Covington, LA). Sixteen Indian-origin rhesus macaques *(Macaca mulatta)* were infected with low dose ~10 colony-forming units (CFUs) of *Mtb* CDC1551 (BEI resources, Cat# NR13649, Manassas, VA) via an aerosol route. Animals were enrolled from a specific pathogen-free colony maintained at TNPRC and were tested free from SPF-4 (simian retrovirus D, SIV, STLV-1 and herpes B virus) and tuberculosis pathogens. A PCR-based molecular typing was performed to study the expression of major histocompatibility class MHC class 1 alleles, MAMU A*01, B*08, B*17, though

enrollment in the study was independent of the MAMU status. All animals reported positive tuberculin skin test (TST) after 3 weeks of exposure, confirming infection. Animals were then followed by weekly physical examination, including body temperature and weight collection and physical examination by a board-certified veterinary clinician. Blood examination, consisting of hematology and serum biochemistry, was performed weekly whereas bronchoalveolar lavage (BAL) was performed biweekly under general anesthesia. Latent TB infection was confirmed if the animals did not show signs of reactivation viz. fever, >20% weight loss, anorexia, labored breathing, and/or raised CRP until week 8 post of *Mtb* exposure. At week 9 post *Mtb* infection, LTBI confirmed animals (n=12) were challenged with 300 $TCID_{50}$ $SIVmac_{239}$ (Preston Marx Lab, TNPRC, Covington, LA) via intravenous route while (n=4) served as LTBI controls. Once infection with SIV was confirmed with plasma SIV RNA viral load animals were randomized to control (ART-naïve) group n=8 and treatment (ART) group n=4. At 13 weeks post *Mtb* infection, treatment group animals were administered combined antiretroviral therapy (cART) regimen. All animals were euthanized by week 24, which was a predetermined study endpoint or at earlier timepoints if the animals were clinically unwell and/or showed signs of TB reactivation, as determined by veterinarians, adhering to humane endpoints criteria.

ART drug formulation

PMPA and FTC were obtained from Gilead Sciences (Foster City, CA) and DTG from ViiV Healthcare (Research Triangle, NC). These antiretroviral drugs were administered in a formulation of 3 drug cocktail dissolved in a vehicle kleptose following published doses for each drug. Each ml of formulation contained two reverse transcriptase inhibitors 20 mg ml^{-1}, tenofovir disoproxil (PMPA) (50-52), 30 mg ml^{-1} emtricitabine (FTC) (53) and an integrase inhibitor 2.5 mg ml^{-1} dolutegravir (DTG) (54, 55).

Plasma and BAL SIV viral load

To determine the efficacy of cART, bronchoalveolar lavage (BAL) samples were collected biweekly by vigorously infusing 50 ml of sterile PBS through an orotracheal tube and aspirating as much of instilled volume as possible. The procedure was performed by trained veterinarians. The aspirated fluid was mixed to 10% FBS v/v during the transit. BAL supernatant (acellular) was stored at -80 C until analysis. Plasma and BAL SIV viral loads were determined in acellular BAL supernatant by RNA extraction and subsequent reverse transcription-polymerase chain reaction (RT-qPCR) using probe targeting the gag gene of SIV. Plasma and BAL SIV viral loads were performed at the NIAID DAIDS Nonhuman Primate Core Virology Laboratory for AIDS Vaccine Research and Development at Duke University, Durham, NC (contract # HHSN272201800003C). The lower limit of quantification for SIV copies in the RNA in this assay is 100 copies/sample.

***In Situ* Hybridization Assay-RNAscope**

Rhesus macaque lungs, bronchial lymph nodes, and spleen tissues were collected during necropsy immediately following euthanasia. Serial sections were prepared from formalin-fixed, paraffin-embedded tissue blocks and used for *In Situ* Hybridization (ISH) using RNAscope 2.5 HD reagent kit (Catalog # 322350, Advanced Cell Diagnostics, Newark, CA) exactly as per the manufacturer's instructions. A SIVmac239 specific probe (Catalog # 312811, Advanced Cell Diagnostics) containing 83 ZZ pairs complementary to the transcripts coded by viral genome region 1251 – 9420 (GenBank: D01065.1) (56) which code for multiple SIV proviral genes (gag, vif, pol, tat, env, vpx, vpr, nef, rev) was used. An identical assay using a probe for bacterial DapB gene (Catalog

320751, Advanced Cell Diagnostics) which is not expressed in mammalian tissues was used as a negative control. Positive signals were detected by counting the number of dots per cell labeled with red dyes, and images were captured using Olympus BX46 microscope with Olympus DP27 camera (Olympus America, Center Valley, PA). A semi-quantitative scoring system based on the manufacturer's recommendation (57), was used to compare the gene expression.

Confocal microscopy

Formalin-fixed and paraffin-embedded (FFPE) sections from the lung, spleen, and lymph nodes harvested at endpoint were stained with H&E, fluorescent immunohistochemistry, and in-situ hybridization as described (44, 58).

Tissue processing and flow cytometry

High parameter flow cytometry was performed on whole blood and BAL samples collected on timepoints weeks 3, 7, 11, 15, 19 and also on lung, BrLN, spleen, granuloma tissues harvested at endpoints, as previously described (15, 18, 21). Briefly, T cell phenotypes were studied using antibodies: CD3 (clone SP34-2), CD4 (clone L200), CD8 (clone RPA-T8), CD69 (clone FN50), CXCR3 (clone 1C6/CXCR3), CCR6 (clone 11A9), HLA-DR (clone L243), PD-1 (clone EH12.2H7, Biolegend, San Diego, CA, USA) all purchased from BD Biosciences (San Jose , CA, USA) unless specified. Flow cytometry data was analyzed using gating strategies described previously using FlowJo platform (Ashland, OR,USA).

Statistical analyses

Graphs were prepared and statistical comparisons applied using GraphPad Prism version 8 (La Jolla, CA). Various statistical comparisons were performed viz. 2-tailed Student's t-test, one-way or two-way analysis of variance (59) with Tukey's or Sidak's multiple comparisons tests wherever

applicable and as described in the figure legends. Statistical differences between groups were reported significant when p-value is less than or equal to 0.05. The data are presented in mean ± SEM.

Author Contributions. S.R.G., A.N.B, S. A. K., S.M., J.R., D.K. designed these studies. S.G., A.N.B., A.C., D.K.S, A.F., T.H.L., X.A., conducted the experiments and acquired the data. S.R.G., R. S., S.M., S.A.K., J.R., D.K., analyzed and interpreted the data and contributed in writing the manuscript.

Acknowledgements. We thank Dr. Preston Marx for sharing a validated stock of SIVmac239. We also thank NIAID DAIDS Nonhuman Primate Core Virology Laboratory for AIDS Vaccine Research and Development contract # HHSN272201800003C for help with SIV viral load assessment. We acknowledge Gilead Sciences for providing drugs PMPA and FTC and ViiV Healthcare for providing DTG.

Financial support. This work was primarily supported by NIH awards to D.K. and J.R. (R01AI111943, R01AI123047) with additional support from NIH awards R01AI111914, R01AI134240, R01AI135726, U19AI111211 and institutional awards P51OD111033 and P51OD111004.

References

1. Spertini F, Audran R, Chakour R, Karoui O, Steiner-Monard V, Thierry AC, et al. Safety of human immunisation with a live-attenuated Mycobacterium tuberculosis vaccine: a randomised, double-blind, controlled phase I trial. *The Lancet Respiratory medicine.* 2015;3(12):953-62.

2. Survival of HIV-positive patients starting antiretroviral therapy between 1996 and 2013: a collaborative analysis of cohort studies. *The lancet HIV.* 2017;4(8):e349-e56.
3. Bor J, Herbst AJ, Newell ML, and Barnighausen T. Increases in adult life expectancy in rural South Africa: valuing the scale-up of HIV treatment. *Science.* 2013;339(6122):961-5.
4. Meintjes G, Brust JCM, Nuttall J, and Maartens G. Management of active tuberculosis in adults with HIV. *The lancet HIV.* 2019;6(7):e463-e74.
5. Etard JF, Ndiaye I, Thierry-Mieg M, Gueye NF, Gueye PM, Laniece I, et al. Mortality and causes of death in adults receiving highly active antiretroviral therapy in Senegal: a 7-year cohort study. *AIDS (London, England).* 2006;20(8):1181-9.
6. Moore D, Liechty C, Ekwaru P, Were W, Mwima G, Solberg P, et al. Prevalence, incidence and mortality associated with tuberculosis in HIV-infected patients initiating antiretroviral therapy in rural Uganda. *AIDS (London, England).* 2007;21(6):713-9.
7. Narita M, Ashkin D, Hollender ES, and Pitchenik AE. Paradoxical worsening of tuberculosis following antiretroviral therapy in patients with AIDS. *American journal of respiratory and critical care medicine.* 1998;158(1):157-61.
8. Lawn SD, Bekker LG, and Miller RF. Immune reconstitution disease associated with mycobacterial infections in HIV-infected individuals receiving antiretrovirals. *The Lancet Infectious diseases.* 2005;5(6):361-73.
9. Suthar AB, and Barnighausen T. Antiretroviral therapy and population mortality: Leveraging routine national data to advance policy. *PLoS Med.* 2017;14(12):e1002469.
10. Gupta A, Wood R, Kaplan R, Bekker LG, and Lawn SD. Tuberculosis incidence rates during 8 years of follow-up of an antiretroviral treatment cohort in South Africa: comparison with rates in the community. *PLoS One.* 2012;7(3):e34156.
11. Khaitan A, and Unutmaz D. Revisiting immune exhaustion during HIV infection. *Curr HIV/AIDS Rep.* 2011;8(1):4-11.
12. Day CL, Kaufmann DE, Kiepiela P, Brown JA, Moodley ES, Reddy S, et al. PD-1 expression on HIV-specific T cells is associated with T-cell exhaustion and disease progression. *Nature.* 2006;443(7109):350-4.
13. Macatangay BJC, Gandhi RT, Jones RB, McMahon DK, Lalama CM, Bosch RJ, et al. T cells with high PD-1 expression are associated with lower HIV-specific immune responses despite long-term antiretroviral therapy. *AIDS.* 2020;34(1):15-24.
14. Lanjewar DN, and Duggal R. Pulmonary pathology in patients with AIDS: an autopsy study from Mumbai. *HIV Med.* 2001;2(4):266-71.
15. Foreman TW, Mehra S, LoBato DN, Malek A, Alvarez X, Golden NA, et al. CD4+ T-cell-independent mechanisms suppress reactivation of latent tuberculosis in a macaque model of HIV coinfection. *Proc Natl Acad Sci U S A.* 2016;113(38):E5636-44.
16. Diedrich CR, Mattila JT, Klein E, Janssen C, Phuah J, Sturgeon TJ, et al. Reactivation of latent tuberculosis in cynomolgus macaques infected with SIV is associated with early peripheral T cell depletion and not virus load. *PLoS One.* 2010;5(3):e9611.
17. Mehra S, Golden NA, Dutta NK, Midkiff CC, Alvarez X, Doyle LA, et al. Reactivation of latent tuberculosis in rhesus macaques by coinfection with simian immunodeficiency virus. *J Med Primatol.* 2011;40(4):233-43.

18. Foreman TW, Bucsan AN, Mehra S, Peloquin C, Doyle LA, Russell-Lodrigue K, et al. Isoniazid and Rifapentine Treatment Eradicates Persistent Mycobacterium tuberculosis in Macaques. *Am J Respir Crit Care Med.* 2019.
19. Bucsan AN, Chatterjee A, Singh DK, Foreman TW, Lee TH, Threeton B, et al. Mechanisms of reactivation of latent tuberculosis infection due to SIV coinfection. *The Journal of clinical investigation.* 2019.
20. Kuroda MJ, Sugimoto C, Cai Y, Merino KM, Mehra S, Arainga M, et al. High Turnover of Tissue Macrophages Contributes to Tuberculosis Reactivation in Simian Immunodeficiency Virus-Infected Rhesus Macaques. *The Journal of infectious diseases.* 2018;217(12):1865-74.
21. Bucsan AN, Chatterjee A, Singh DK, Foreman TW, Lee TH, Threeton B, et al. Mechanisms of reactivation of latent tuberculosis infection due to SIV coinfection. *J Clin Invest.* 2019;129(12):5254-60.
22. Foreman TW, Veatch AV, LoBato DN, Didier PJ, Doyle-Meyers LA, Russell-Lodrigue KE, et al. Nonpathologic Infection of Macaques by an Attenuated Mycobacterial Vaccine Is Not Reactivated in the Setting of HIV Co-Infection. *The American journal of pathology.* 2017;187(12):2811-20.
23. Whitney JB, Hill AL, Sanisetty S, Penaloza-MacMaster P, Liu J, Shetty M, et al. Rapid seeding of the viral reservoir prior to SIV viraemia in rhesus monkeys. *Nature.* 2014;512(7512):74-7.
24. Fuller CL, Choi YK, Fallert BA, Capuano S, 3rd, Rajakumar P, Murphey-Corb M, et al. Restricted SIV replication in rhesus macaque lung tissues during the acute phase of infection. *Am J Pathol.* 2002;161(3):969-78.
25. Li Y, Kang G, Duan L, Lu W, Katze MG, Lewis MG, et al. SIV Infection of Lung Macrophages. *PLoS One.* 2015;10(5):e0125500.
26. Barry CE, 3rd, Boshoff HI, Dartois V, Dick T, Ehrt S, Flynn J, et al. The spectrum of latent tuberculosis: rethinking the biology and intervention strategies. *Nat Rev Microbiol.* 2009;7(12):845-55.
27. McBride A, Konowich J, and Salgame P. Host defense and recruitment of Foxp3(+) T regulatory cells to the lungs in chronic Mycobacterium tuberculosis infection requires toll-like receptor 2. *PLoS Pathog.* 2013;9(6):e1003397.
28. Corleis B, Bucsan AN, Deruaz M, Vrbanac VD, Lisanti-Park AC, Gates SJ, et al. HIV-1 and SIV Infection Are Associated with Early Loss of Lung Interstitial CD4+ T Cells and Dissemination of Pulmonary Tuberculosis. *Cell reports.* 2019;26(6):1409-18 e5.
29. Pallikkuth S, Fischl MA, and Pahwa S. Combination antiretroviral therapy with raltegravir leads to rapid immunologic reconstitution in treatment-naive patients with chronic HIV infection. *J Infect Dis.* 2013;208(10):1613-23.
30. Reiley WW, Calayag MD, Wittmer ST, Huntington JL, Pearl JE, Fountain JJ, et al. ESAT-6-specific CD4 T cell responses to aerosol Mycobacterium tuberculosis infection are initiated in the mediastinal lymph nodes. *Proc Natl Acad Sci U S A.* 2008;105(31):10961-6.
31. Khoury G, Anderson JL, Fromentin R, Hartogenesis W, Smith MZ, Bacchetti P, et al. Persistence of integrated HIV DNA in CXCR3 + CCR6 + memory CD4+ T cells in HIV-infected individuals on antiretroviral therapy. *AIDS.* 2016;30(10):1511-20.

32. Silveira-Mattos PS, Narendran G, Akrami K, Fukutani KF, Anbalagan S, Nayak K, et al. Differential expression of CXCR3 and CCR6 on CD4(+) T-lymphocytes with distinct memory phenotypes characterizes tuberculosis-associated immune reconstitution inflammatory syndrome. *Sci Rep.* 2019;9(1):1502.
33. O'Garra A, Redford PS, McNab FW, Bloom CI, Wilkinson RJ, and Berry MP. The immune response in tuberculosis. *Annu Rev Immunol.* 2013;31:475-527.
34. Marin ND, Dunlap MD, Kaushal D, and Khader SA. Friend or Foe: The Protective and Pathological Roles of Inducible Bronchus-Associated Lymphoid Tissue in Pulmonary Diseases. *J Immunol.* 2019;202(9):2519-26.
35. Moyron-Quiroz JE, Rangel-Moreno J, Hartson L, Kusser K, Tighe MP, Klonowski KD, et al. Persistence and responsiveness of immunologic memory in the absence of secondary lymphoid organs. *Immunity.* 2006;25(4):643-54.
36. Rangel-Moreno J, Hartson L, Navarro C, Gaxiola M, Selman M, and Randall TD. Inducible bronchus-associated lymphoid tissue (iBALT) in patients with pulmonary complications of rheumatoid arthritis. *J Clin Invest.* 2006;116(12):3183-94.
37. Hirahara K, Shinoda K, Morimoto Y, Kiuchi M, Aoki A, Kumagai J, et al. Immune Cell-Epithelial/Mesenchymal Interaction Contributing to Allergic Airway Inflammation Associated Pathology. *Front Immunol.* 2019;10:570.
38. Picker LJ, Reed-Inderbitzin EF, Hagen SI, Edgar JB, Hansen SG, Legasse A, et al. IL-15 induces CD4 effector memory T cell production and tissue emigration in nonhuman primates. *J Clin Invest.* 2006;116(6):1514-24.
39. Kaushal D, Foreman TW, Gautam US, Alvarez X, Adekambi T, Rangel-Moreno J, et al. Mucosal vaccination with attenuated Mycobacterium tuberculosis induces strong central memory responses and protects against tuberculosis. *Nat Commun.* 2015;6:8533.
40. Abreu CM, Veenhuis RT, Avalos CR, Graham S, Queen SE, Shirk EN, et al. Infectious Virus Persists in CD4(+) T Cells and Macrophages in Antiretroviral Therapy-Suppressed Simian Immunodeficiency Virus-Infected Macaques. *J Virol.* 2019;93(15).
41. Ortiz AM, Klatt NR, Li B, Yi Y, Tabb B, Hao XP, et al. Depletion of CD4(+) T cells abrogates post-peak decline of viremia in SIV-infected rhesus macaques. *J Clin Invest.* 2011;121(11):4433-45.
42. Clayton KL, Collins DR, Lengieza J, Ghebremichael M, Dotiwala F, Lieberman J, et al. Resistance of HIV-infected macrophages to CD8(+) T lymphocyte-mediated killing drives activation of the immune system. *Nat Immunol.* 2018;19(5):475-86.
43. Diedrich CR. SIV and Mycobacterium tuberculosis synergy within the granuloma accelerates the reactivation pattern of
2 latent tuberculosis. 2020.
44. Gautam US, Foreman TW, Bucsan AN, Veatch AV, Alvarez X, Adekambi T, et al. In vivo inhibition of tryptophan catabolism reorganizes the tuberculoma and augments immune-mediated control of Mycobacterium tuberculosis. *Proc Natl Acad Sci U S A.* 2018;115(1):E62-E71.
45. Namale PE, Abdullahi LH, Fine S, Kamkuemah M, Wilkinson RJ, and Meintjes G. Paradoxical TB-IRIS in HIV-infected adults: a systematic review and meta-analysis. *Future Microbiol.* 2015;10(6):1077-99.

46. Sterling TR, Alwood K, Gachuhi R, Coggin W, Blazes D, Bishai WR, et al. Relapse rates after short-course (6-month) treatment of tuberculosis in HIV-infected and uninfected persons. *AIDS.* 1999;13(14):1899-904.
47. van Rie A, Warren R, Richardson M, Victor TC, Gie RP, Enarson DA, et al. Exogenous reinfection as a cause of recurrent tuberculosis after curative treatment. *N Engl J Med.* 1999;341(16):1174-9.
48. Rangaka MX, Wilkinson RJ, Boulle A, Glynn JR, Fielding K, van Cutsem G, et al. Isoniazid plus antiretroviral therapy to prevent tuberculosis: a randomised double-blind, placebo-controlled trial. *Lancet.* 2014;384(9944):682-90.
49. Group TAS, Danel C, Moh R, Gabillard D, Badje A, Le Carrou J, et al. A Trial of Early Antiretrovirals and Isoniazid Preventive Therapy in Africa. *N Engl J Med.* 2015;373(9):808-22.
50. Tsai CC, Follis KE, Sabo A, Beck TW, Grant RF, Bischofberger N, et al. Prevention of SIV infection in macaques by (R)-9-(2-phosphonylmethoxypropyl)adenine. *Science (New York, NY).* 1995;270(5239):1197-9.
51. Silvera P, Racz P, Racz K, Bischofberger N, Crabbs C, Yalley-Ogunro J, et al. Effect of PMPA and PMEA on the kinetics of viral load in simian immunodeficiency virus-infected macaques. *AIDS research and human retroviruses.* 2000;16(8):791-800.
52. Mavigner M, Habib J, Deleage C, Rosen E, Mattingly C, Bricker K, et al. Simian Immunodeficiency Virus Persistence in Cellular and Anatomic Reservoirs in Antiretroviral Therapy-Suppressed Infant Rhesus Macaques. *Journal of virology.* 2018;92(18).
53. Klatt NR, Shudo E, Ortiz AM, Engram JC, Paiardini M, Lawson B, et al. CD8+ lymphocytes control viral replication in SIVmac239-infected rhesus macaques without decreasing the lifespan of productively infected cells. *PLoS pathogens.* 2010;6(1):e1000747.
54. Del Prete GQ, Smedley J, Macallister R, Jones GS, Li B, Hattersley J, et al. Short Communication: Comparative Evaluation of Coformulated Injectable Combination Antiretroviral Therapy Regimens in Simian Immunodeficiency Virus-Infected Rhesus Macaques. *AIDS research and human retroviruses.* 2016;32(2):163-8.
55. Van Rompay KKA, Hassounah S, Keele BF, Lifson JD, Ardeshir A, Watanabe J, et al. Dolutegravir Monotherapy of Simian Immunodeficiency Virus-Infected Macaques Selects for Several Patterns of Resistance Mutations with Variable Virological Outcomes. *Journal of virology.* 2019;93(2).
56. GenBank. D01065.1: Simian immunodeficiency virus proviral gag, vif, pol, tat, env, vpx, vpr, nef, rev genes, complete and partial cds. https://www.ncbi.nlm.nih.gov/nuccore/D01065.1.
57. Acdbio. Advanced cell diagnostic, RNAscope technical guide. https://acdbio.com/technical-support/solutions.
58. Gautam US, McGillivray A, Mehra S, Didier PJ, Midkiff CC, Kissee RS, et al. DosS Is required for the complete virulence of mycobacterium tuberculosis in mice with classical granulomatous lesions. *Am J Respir Cell Mol Biol.* 2015;52(6):708-16.
59. Shcherbo D, Merzlyak EM, Chepurnykh TV, Fradkov AF, Ermakova GV, Solovieva EA, et al. Bright far-red fluorescent protein for whole-body imaging. *Nature methods.* 2007;4(9):741-6.

Figure legends

Figure 1. Clinical correlates of TB reactivation in ART-treated NHPs with *Mtb/SIV* co-infection: (A) Study outline. Sixteen Indian origin rhesus macaques infected with low-dose *Mtb* CDC1551 via aerosol route developed latent TB. At week 9 post *Mtb* challenge, some of these NHPs (n=12) were challenged with intravenous infection of *SIVmac239*. At week 13, of the twelve *Mtb/SIV* co-infected NHPs (n=4) received *ART* regimen while n=8 served as ART-naïve controls. Animals with TB reactivation and signs of disease had to undergo an early necropsy to meet the humane endpoints criteria set by TNPRC IACUC committee, while animals with no signs of active disease were necropsied by week 24 (B) Plasma viral loads were measured at peak of SIV infection i.e. around week 11 of infection and at the endpoint. (C) Survival curve, X-axis displays times in weeks post *Mtb* infection and Y-axis displays percent survival. (D) Serum C-reactive protein (CRP) levels measured at week 11 and the endpoint. (E) BAL SIV RNA load measured at necropsy (F) RNAscope in-situ hybridization assay was used to examine the presence of SIV RNA in tissues like lung, BrLN, and spleen. ART treatment substantially reduced the viral particles, vRNA+ cells (red), in spleen and BrLN tissue whereas the changes were not appreciable in the sparsely infected lung parenchyma. The three groups studied are *Mtb* infection only i.e. LTBI (n=4, green), *Mtb/SIV* co-infection i.e. ART-naïve (n=8, red) and *Mtb/SIV* co-infection with ART treatment i.e. ART (n=4, blue); (B, D, E) data represented as mean±SEM; (C) log-rank test (Mantel-Cox) used to compare survival curves; (D) two-way ANOVA with Sidak's multiple comparison test and (B, E) two-tailed Student's t-test; *$P < 0.05$; **$P < 0.01$; ***$P < 0.001$; ****$P < 0.0001$. The error bars in the dot plot represent the standard error of the mean (SEM)

Figure 1.

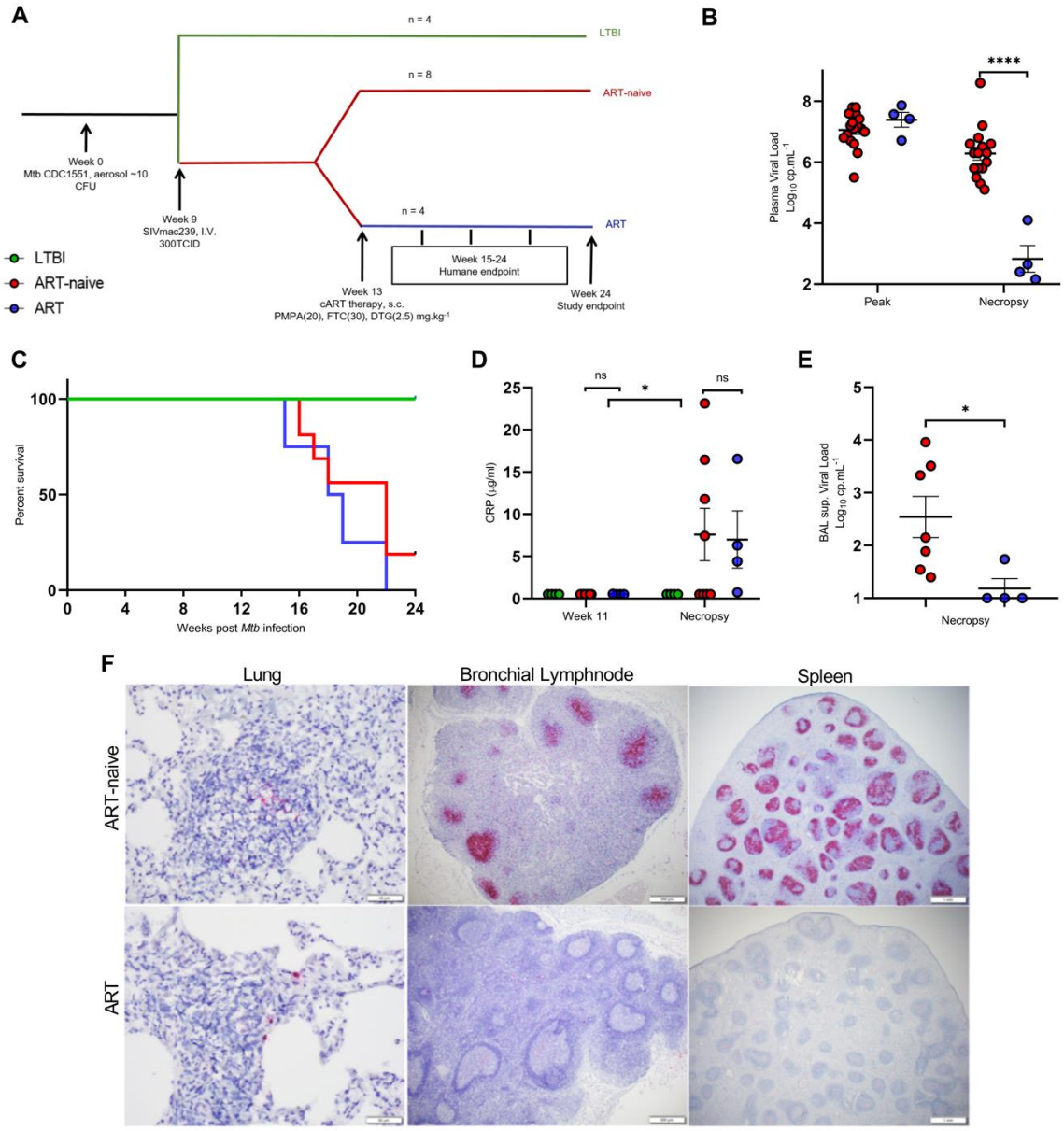
A
n = 4
LTBI
n = 8
ART-naive
n = 4
ART
Week 0
Mtb CDC1551, aerosol ~10 CFU
Week 9
SIVmac239, I.V. 300TCID
Week 13
cART therapy, s.c.
PMPA(20), FTC(30), DTG(2.5) mg.kg-1
Week 15-24
Humane endpoint
Week 24
Study endpoint
LTBI
ART-naive
ART
B
****
Plasma Viral Load
Log10 cp.mL-1
Peak
Necropsy
C
Percent survival
Weeks post Mtb infection
D
ns
*
ns
CRP (µg/ml)
Week 11
Necropsy
E
*
BAL sup. Viral Load
Log10 cp.mL-1
Necropsy
F
Lung
Bronchial Lymphnode
Spleen
ART-naive
ART

Figure 2. *Mtb* bacterial burden and lung pathology. *Mtb* bacterial burden was obtained by normalizing the CFU counts to log-transformed CFU per gram of tissue. (A) *Mtb* CFUs in total BAL sample (cellular + acellular component); (B) *Mtb* CFU count normalized to per gram of lung tissue collected at necropsy; (C) Multiple granulomas (n= 1-6) per animal were grouped as per the experimental classification of the animal; each granuloma was weighed and its CFU count normalized to per gram of granuloma tissue; (D) BrLN; (E) Spleen; (F) percent lung involvement was calculated by pathologists through extensive analysis of serially cut fresh lung samples and counting no. of lesions in low power magnification. (G) Gross pathology and H&E staining portray the large granulomatous and necrotic lesions in animals with SIV induced *Mtb* reactivation while minimal pathology seen in samples from latent TB animals. The three groups studied are *Mtb* infection only i.e. LTBI (n=4, shown in green), *Mtb*/SIV co-infection i.e. ART-naïve (n=8, shown in red) and *Mtb*/SIV co-infection with ART treatment i.e. ART (n=4, shown in blue).(A-F) data represented as mean±SEM; (A-F) One-way ANOVA with Tukey's multiple comparison test;*P < 0.05; **P < 0.01; ***P < 0.001; ****P < 0.0001. The error bars in the dot plot represent the standard error of the mean (SEM)

630 **Figure 2.**

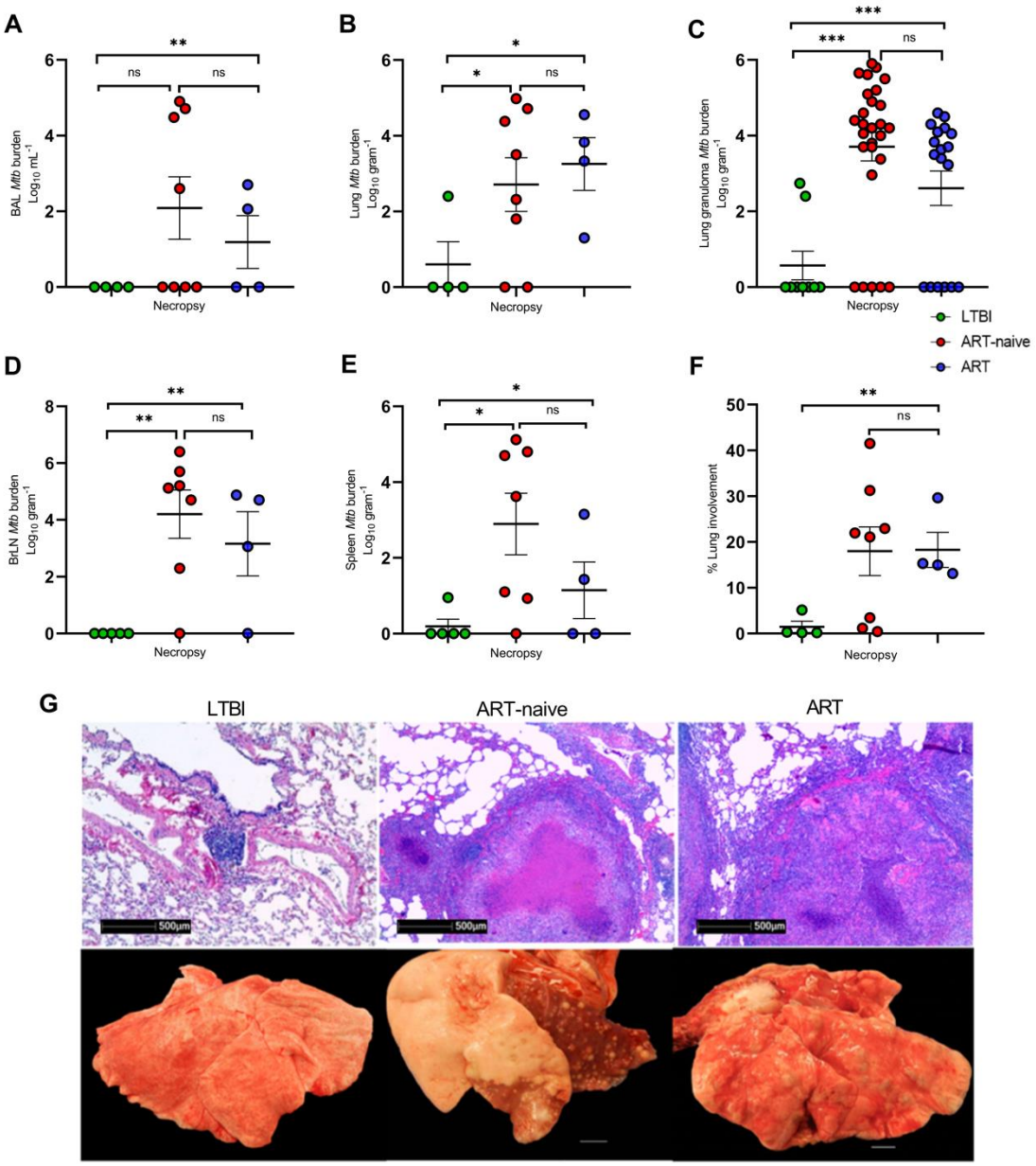

631
632

Figure 3. Differential $CD4^+$ T cell restoration in alveolar and interstitial compartments after ART therapy in *Mtb/SIV* co-infection of NHPs. Multiparameter flow cytometry was performed on single-cell suspension of various tissue samples and whole blood collected at necropsy from *Mtb/SIV* co-infected rhesus macaques treated with ART. The three groups studied are *Mtb* infection only i.e. LTBI (n=4, green), *Mtb*/SIV co-infection i.e. ART-naïve (n=8, red) and *Mtb*/SIV co-infection with ART treatment i.e. ART (n=4, blue). $CD4^+$ T cell frequency was analyzed in (A) whole blood, (B) BAL, (C) lung, (D) Br. LN, (E) spleen. (F) confocal microscopy of formalin-fixed and paraffin-embedded (FFPE) sections from lungs harvested at the endpoint of LTBI (n=3), ART-naïve (n=6), and ART (n=3) treated macaques reports the $CD4^+$ T cells (CD4/nuclei) in lung tissue sections, counted using HALO™ image analysis software. (G) represent $CD4^+$ T cell (red), $CD68^+CD163^+$ macrophage (green), nucleus (grey), autofluorescent RBCs (yellow), and white arrowheads indicate macrophages phagocytosing $CD4^+$ T cells in the lungs of LTBI, ART-naïve and ART groups respectively. (A-F) data represented as mean±SEM; (A-F) one-way ANOVA with Tukey's multiple comparison test; *P < 0.05; **P < 0.01; ***P < 0.001; ****P < 0.0001. The error bars in the dot plot represent the standard error of the mean (SEM).

Figure 3.

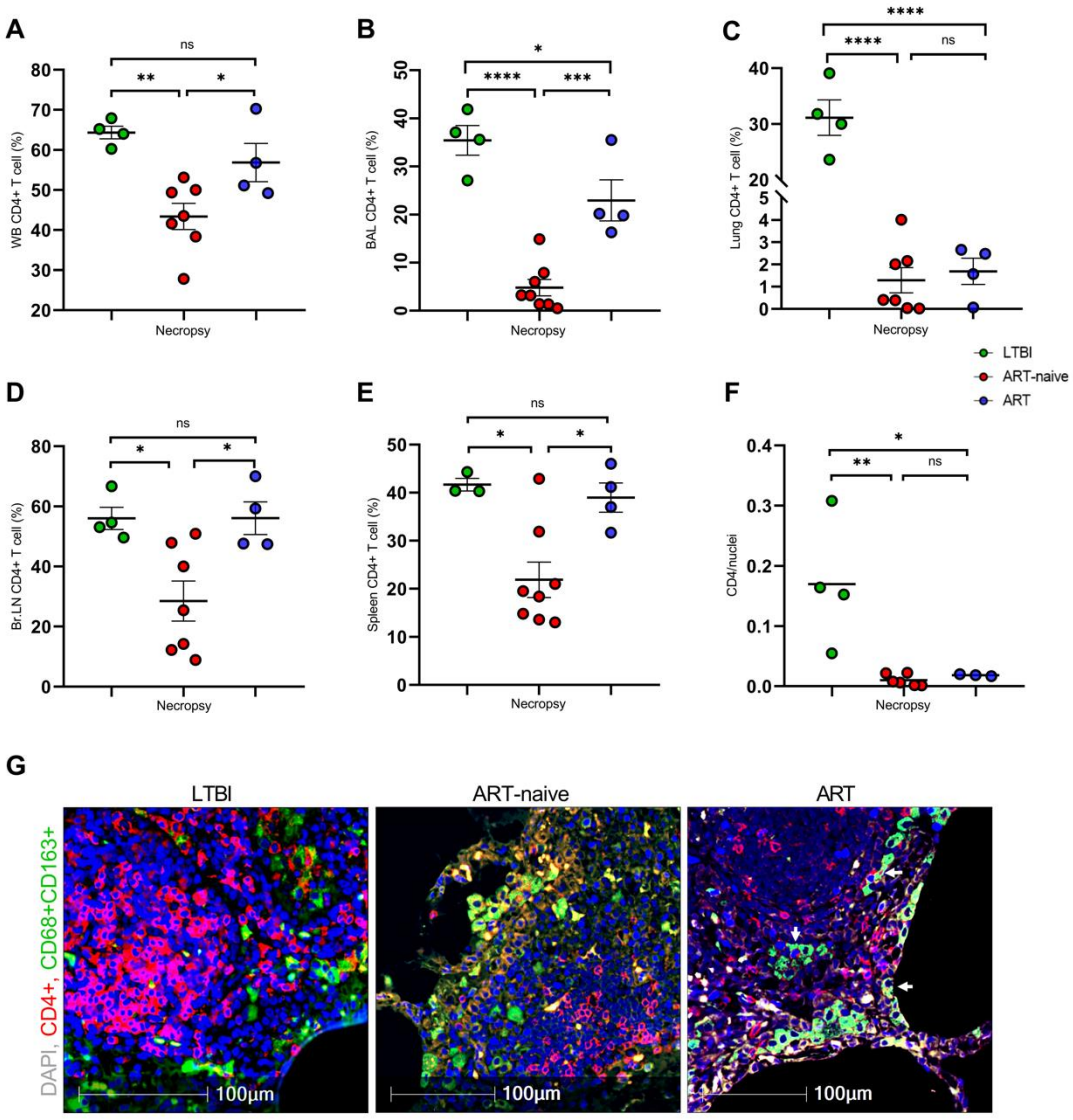
A
B
C
D
E
F
G
WB CD4+ T cell (%)
BAL CD4+ T cell (%)
Lung CD4+ T cell (%)
Br.LN CD4+ T cell (%)
Spleen CD4+ T cell (%)
CD4/nuclei
Necropsy
ns
LTBI
ART-naive
ART
DAPI, CD4+, CD68+CD163+
100µm

Figure 4. Dysregulation in homing of $CD4^+$ T cells to iBALT in lung interstitium of *Mtb/SIV* co-infected macaques. Immunohistochemistry staining and confocal imaging of formalin-fixed, paraffin-embedded (FFPE) lung sections from *Mtb/SIV* infected macaques with/without ART. The figure is representative of three experimental replicates. (**A**) Nuclei/DAPI (grey), SIV RNA^+ (red), $CD3^+$ T lymphocytes (blue) and $CD68^+CD163^+$ macrophages (green) identify macrophages phagocytosing $vRNA^+$ cells present in the iBALT. (**B**) Nuclei/DAPI (grey), IDO1 expressing cells (red), $CD20^+$ B lymphocytes (blue) and $CD68^+CD163^+$ macrophages (green) identify well-organized B cell zones of iBALT and presence of IDO1 expressing macrophages in the T cell zone of the iBALT. (C**)** Nuclei/DAPI (grey), IDO1 expressing cells (red), and $CD68^+CD163^+$ macrophages (green) of granuloma in *Mtb*/SIV co-infected animal showing that majority of the IDO1 expression is seen in $CD68^+CD163^+$ macrophage rich layer of granulomas in macaques with TB reactivation. (D) Nuclei/DAPI (blue), IDO1 expressing cells (green), and $CD141^+$ tolerogenic dendritic cells (red), shows IDO1 expression by dendritic cells. The IHC staining was performed on sections of the lungs from macaques with Mtb infection only i.e. LTBI (n=3), Mtb/SIV co-infection i.e. ART-naïve (n=3) and Mtb/SIV co-infection with ART treatment i.e. ART (n=3) groups.

Figure 4.

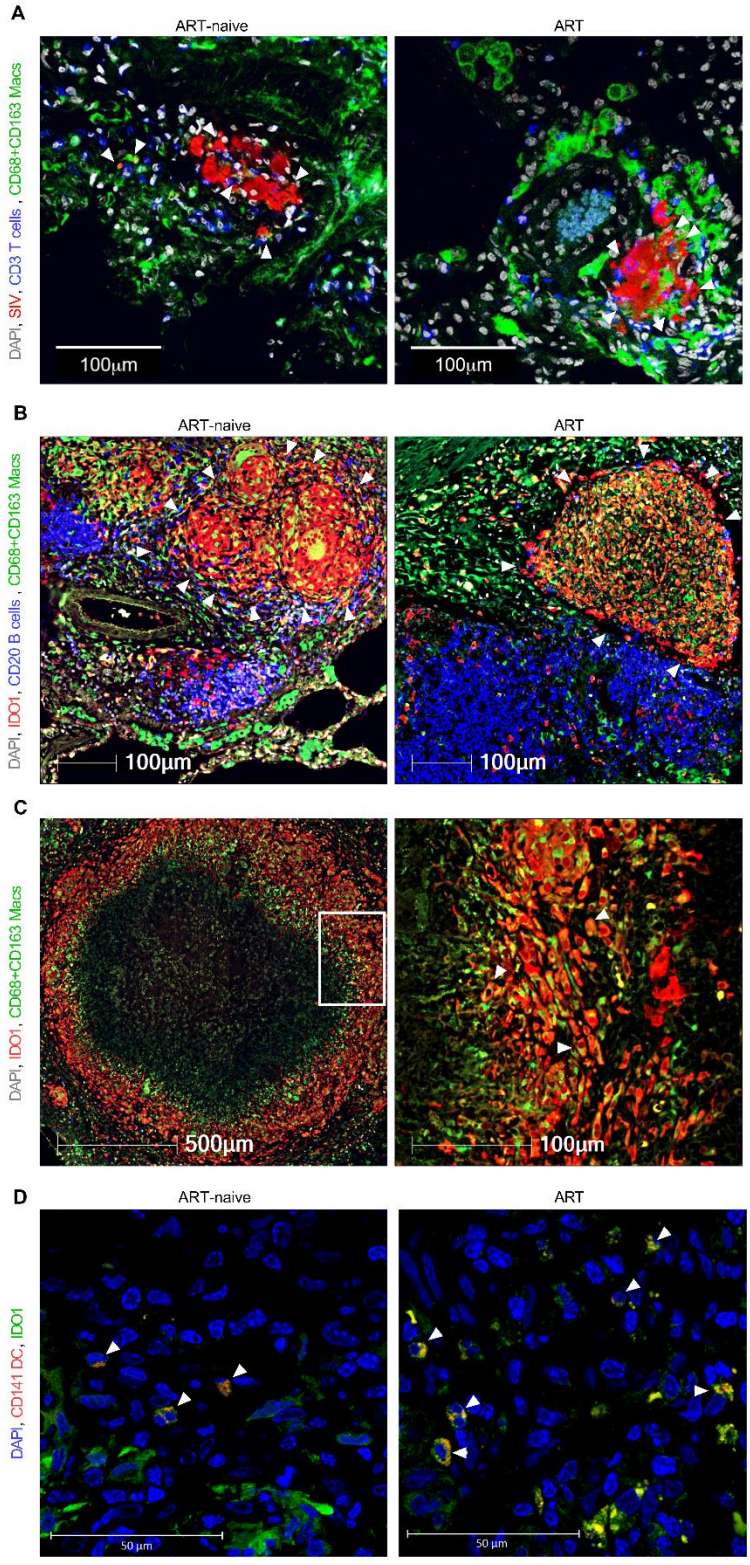
A
ART-naive
ART
DAPI, SIV, CD3 T cells , CD68+CD163 Macs
100µm
100µm
B
ART-naive
ART
DAPI, IDO1, CD20 B cells , CD68+CD163 Macs
100µm
100µm
C
DAPI, IDO1, CD68+CD163 Macs
500µm
100µm
D
ART-naive
ART
DAPI, CD141 DC, IDO1
50 µm
50 µm